ARMY RESEARCH LABORATORY

Computational Modeling of a Finned Projectile by Chimera Technique

Harris L. Edge
Jubaraj Sahu

ARL-TR-1443 DECEMBER 1997

19980113 008

DTIC QUALITY INSPECTED 3

Abstract

A computational study was performed to compute the aerodynamic coefficients of a long-range finned projectile configuration at a transonic velocity of Mach 0.95 for multiple angles of attack. A zonal, implicit, Navier-Stokes computational technique, along with the Chimera overset grid approach, has been used to compute the projectile flow field. The application of the Chimera approach allowed for improved efficiency in terms of placing grid points where they are needed the most. This technique is promising for future flow field computations of finned projectiles. The aerodynamic coefficients computed are then compared with those computed through application of a design code to show comparable results.

ACKNOWLEDGMENTS

INTENTIONALLY LEFT BLANK

TABLE OF CONTENTS

INTENTIONALLY LEFT BLANK

LIST OF FIGURES

INTENTIONALLY LEFT BLANK

LIST OF TABLES

INTENTIONALLY LEFT BLANK

COMPUTATIONAL MODELING OF A FINNED
PROJECTILE BY CHIMERA TECHNIQUE

1. INTRODUCTION

The Aerodynamics Branch, Propulsion and Flight Division, Weapons and Materials Research Directorate of the U.S. Army Research Laboratory (ARL) has made a concerted effort to develop sophisticated predictive capabilities for aerodynamic coefficients of U.S. Army artillery, based on the solution of the Navier-Stokes equations through computational fluid dynamics (CFD). Recently, the efforts have focused on establishing the capability to predict control aerodynamics of such devices as canards and fins associated with smart munitions and missile and rocket systems. These are areas of interest to U.S. Army (the U.S. Army Armament Research, Development, and Engineering Center [ARDEC] and U.S. Army Missile Command [MICOM]), Air Force, and Navy programs. Eventually, these CFD developments will be integrated in an effort to develop a multidisciplinary design capability for complex U.S. Army smart munitions systems.

As a step toward this goal, CFD computations have been performed for a proposed U.S. Army projectile at moderate angles of attack at a transonic velocity where aerodynamic coefficients can be inherently nonlinear. Obtaining accurate predictions of aerodynamics coefficients during these conditions is crucial to simulate flight trajectories of smart munitions. The method of performing this computation was conceived to not only perform this series of computations but to also be adaptive enough to be applicable to a number of potential future missile designs. Overset grid discretization was employed in order to provide the grid density required for a quality viscous Navier-Stokes solution and yet keep the number of grid points to a manageable number for operating the CFD solver on a standard supercomputer. In the future, this technique will be extended to include the modeling of canards and other aerodynamic control devices. The modeling of complex shapes can be greatly simplified through the use of overset grid discretization techniques. Verification of this technique as a viable means to routinely obtain aerodynamic coefficients of complex missiles is a key accomplishment gained while performing the CFD computations.

The computations also provide a basis of comparison for aerodynamic coefficients obtained by design code methodology. This is important because the CFD computations are costly in terms of time and effort in comparison to those of a design code. However,

for complex missiles, at high angles of attack, design code-obtained aerodynamic coefficients may not be reliable. The aerodynamic coefficients obtained from the CFD computations will be compared with those obtained from design codes in order to ascertain their applicability in this flight regime. The knowledge gained from the CFD computations may also be used to improve the methodology employed for application of design codes.

2. GOVERNING EQUATIONS AND SOLUTION TECHNIQUE

The complete set of time-dependent, Reynolds-averaged, thin layer, Navier-Stokes equations is solved numerically to obtain a solution to this problem. The numerical technique used is an implicit, finite difference scheme. Steady state calculations are made to numerically compute the flow field for a finned projectile.

2.1 Governing Equations

The complete set of three-dimensional (3-D), time-dependent, generalized geometry, Reynolds-averaged, thin layer, Navier-Stokes equations for general spatial coordinates ξ, η, and ζ can be written as follows (Pulliam & Steger 1982):

$$\partial_\tau \hat{q} + \partial_\xi \hat{F} + \partial_\eta \hat{G} + \partial_\zeta \hat{H} = Re^{-1} \partial_\zeta \hat{S}, \tag{1}$$

in which

$$\xi = \xi(x, y, z, t) \text{ - longitudinal coordinate;}$$
$$\eta = \eta(x, y, z, t) \text{ - circumferential coordinate}$$
$$\zeta = \zeta(x, y, z, t) \text{ - nearly normal coordinate;}$$
$$\tau = t \text{ - time}$$

In Equation (1), $\hat{q}$ contains the dependent variables (density, three velocity components, and the energy), and $\hat{F}, \hat{G},$ and $\hat{H}$ are flux vectors. The thin layer approximation is used here, and the viscous terms involving velocity gradients in both the longitudinal and circumferential directions are neglected. The viscous terms are retained in the normal direction, ζ, for the projectile and are collected into the vector $\hat{S}$. In the wake or the base region, similar viscous terms are also added in the stream-wise direction, ξ. For computation of turbulent flows, the turbulent contributions are supplied through an algebraic eddy viscosity turbulence model developed by Baldwin and Lomax (1978).

2

2.2 Numerical Technique

The implicit, approximately factored scheme for the thin layer, Navier-Stokes equations using central differencing in the η and ζ directions and upwinding in ξ is written in the following form (see Steger, Ying, & Schiff 1986):

$$\left[I + i_b h \delta_\xi^b \left(\hat{A}^+ \right)^n + i_b h \delta_\zeta \hat{C}^n - i_b h \, Re^{-1} \bar{\delta}_\zeta J^{-1} \hat{M}^n \, J - i_b D_i|_\zeta \right]$$

$$\times \left[I + i_b h \delta_\xi^f \left(\hat{A}^- \right)^n + i_b h \delta_\eta \hat{B}^n - i_b D_i|_\eta \right] \Delta \hat{Q}^n$$

$$= -i_b \Delta t \left\{ \delta_\xi^b \left[\left(\hat{F}^+ \right)^n - \hat{F}_\infty^+ \right] + \delta_\xi^f \left[\left(\hat{F}^- \right)^n - \hat{F}_\infty^- \right] + \delta_\eta \left(\hat{G}^n - \hat{G}_\infty \right) + \delta_\zeta \left(\hat{H}^n - \hat{H}_\infty \right) - Re^{-1} \bar{\delta}_\zeta \left(\hat{S}^n - \hat{S}_\infty \right) \right\}$$

$$- i_b D_e \left(\hat{Q}^n - \hat{Q}_\infty \right), \tag{2}$$

in which $h = \Delta t$ or $(\Delta t)/2$. The free-stream fluxes are subtracted from the governing equation to reduce the possibility of error from the free-stream solution corrupting the converged solution. Here, δ is typically a three-point, second order, accurate central difference operator; $\bar{\delta}$ is a midpoint operator used with the viscous terms; and the operators δ_ξ^b and δ_ξ^f are backward and forward three-point difference operators. The flux $\hat{F}$ has been eigensplit and the matrices $\hat{A}$, $\hat{B}$, $\hat{C}$, and $\hat{M}$ result from local linearization of the fluxes about the previous time level. Here, J denotes the Jacobian of the coordinate transformation. Dissipation operators D_e and D_i are used in the central space differencing directions. The smoothing terms used in the present study are of the form

$$D_e \Big|_\eta = (\Delta t) J^{-1} \left[\varepsilon_2 \bar{\delta} \rho(B) \beta \bar{\delta} + \varepsilon_4 \bar{\delta} \, \frac{\rho(B)}{1+\beta} \, \bar{\delta}^3 \right] \Big|_\eta J,$$

and

$$D_i \Big|_\eta = (\Delta t) J^{-1} \left[\varepsilon_2 \bar{\delta} \rho(B) \beta \bar{\delta} + 2.5 \varepsilon_4 \bar{\delta} \rho(B) \bar{\delta} \right] \Big|_\eta J$$

in which

$$\beta = \frac{\left| \bar{\delta}^2 P \right|}{\left| \left(1 + \delta^2 \right) P \right|}$$

and in which $\rho(B)$ is the true spectral radius of B. The idea here is that the fourth difference will be "tuned down" (i.e., decreased incrementally) near shocks (e.g., as β gets large, the weight on the fourth difference is decreased while the second difference is increased).

3

2.3 Chimera Composite Grid Scheme

The Chimera overset grid scheme is a domain decomposition approach where a configuration is meshed using a collection of overset grids. It allows each component of the configuration to be gridded separately and overset into a main grid. Overset grids are not required to join in any special way. Usually, there is a major grid that covers the entire domain or a grid generated about a dominant body. Minor grids are generated about the rest of the other bodies, which in this case would be fins. This approach was not used in this case. Instead, a basic zonal block structure was used to model the geometry. This allowed the fin body juncture to be modeled accurately without the need for additional complex "collar" grids to be built in order to tie the computational domain of the fin to that of the body. Employing a zonal block structure basically means that the Chimera scheme was used to interpolate and pass information between planes of adjacent zones. It was necessary to employ the Chimera scheme with this type of grid topology because of its ability to pass information between planes of adjacent zones where the grid points were not aligned. Applying the Chimera scheme in this manner also produces the additional benefit of allowing different grid clustering to be used in adjacent zones. Because each component grid is generated independently, portions of one grid may be found to lie within a solid boundary contained within another grid. Such points lie outside the computational domain and are excluded from the solution process.

Within the Chimera scheme, it is possible for the minor grid to be completely overlapped by the major grid; thus, its outer boundary can obtain information by interpolation from the major grid. Similar data transfer or communication is needed from the minor grid to the major grid. However, a natural, outer boundary that overlaps the minor grid does not exist for the major grid. The Chimera technique creates an artificial boundary (also known as a hole boundary) within the major grid that provides the required path for information transfer from the minor grid to the major grid. The resulting hole region is excluded from the flow field solution in the major grid. By using a zonal block structure to model the entire projectile, no grid is completely overlapped by another. Instead, adjacent zones are overlapped by only a couple of planes, and the information transfer is held only to those planes where adjacent zones overlap. Equation (2) has been modified for Chimera overset grids by the introduction of the flag i_b to achieve just that. This i_b array accommodates the possibility of having arbitrary holes in the grid. The i_b array is defined so that $i_b = 1$ at normal grid points and $i_b = 0$ at hole points. Thus, when $i_b = 1$, Equation (2) becomes the standard scheme, but when $i_b = 0$, the algorithm reduces to $\Delta\hat{Q}^n = 0$ or $\hat{Q}^{n+1} = \hat{Q}^n$, leaving $\hat{Q}$ unchanged at hole points. The

4

set of grid points that form the border between the hole points and the normal field points are called inter-grid boundary points. These points are updated by interpolating the solution from the overset grid that created the hole. Values of the i_b array and the interpolation coefficients needed for this update are provided through a separate algorithm developed by Benek, Donegan, and Suhs (1987).

In the present study, only a single body is involved. Since there are no moving parts, the location of the holes and the inter-grid boundary points are not time dependent. Under these circumstances, a zonal block structure is most appropriate. However, if the fin were to be placed in motion relative to the body, such as in a dynamic control surface computation, completely overset fin grids along with the associated "collar" grids would most likely need to be used. The locations of the grid holes and the inter-grid boundary points would be functions of time. Accordingly, the i_b array and the interpolation coefficients would then be functions of time. This procedure of unsteady Chimera decomposition has been successfully demonstrated by Meakin and Suhs (1989). The method depends on three functions: domain connectivity, aerodynamics, and body dynamics. The aerodynamics code depends on the domain connectivity code to supply hole and interpolation information. The domain connectivity code, in turn, depends on the body dynamics code to supply the location and orientation of the moving bodies relative to the primary body. Finally, the body dynamics code depends on the aerodynamics code to provide the aerodynamic forces and moments acting on the moving bodies. The Chimera technique provides a number of options for geometric modeling of complex configurations of which the zonal block model is just one. As the complexity of the configurations increases and the need for dynamic simulations increases, the zonal block model can be further extended through the use of the Chimera technique.

2.4 Domain Connectivity Function

A major part of the Chimera overset grid approach is the information transfer from one grid into another by means of the inter-grid boundary points. Again, these points consist of a set of points that define the hole boundaries and outer boundaries of the minor grids. These points depend on the solutions in the overlapping regions. In the present work, the Domain Connectivity Function in Three Dimensions (DCF3D) Code of Meakin and Suhs (1989) has been used to establish the linkages between the various grids that are required by the flow solver or aerodynamics code described earlier. These include the determination of the interpolation coefficients and the foundation of Chimera logic for bodies making holes in overlapping grids. For unsteady moving grid cases, this

code must be executed at each time iteration. To minimize the computation time, this code uses the knowledge of hole and interpolated boundary points at time level n to limit its search regions for finding their corresponding locations at time level n + 1.

In general, each component grid in an overset grid system represents a curvilinear system of points. However, the position of all points in all the grids are defined relative to an inertial system of reference. To provide domain connectivity, inverse mappings are used that allow easy conversion from x, y, z inertial system to ξ, ζ, η computational space. For moving body problems, these maps for component grids are created only once. Identification of the inter-grid boundary points that correspond to the outer boundaries of the minor grids is done simply by specifying appropriate ranges of coordinate indices. The rest of the inter-grid boundary points that result from holes created by a body in overset grids are a little more difficult to identify. A collection of analytical shapes such as cones, cylinders, and boxes is used to cut holes in this method.

2.5 Boundary Conditions

For simplicity, most of the boundary conditions have been imposed explicitly. An adiabatic wall boundary condition is used on the body surface, and the no-slip boundary condition is used at the wall. The pressure at the wall is calculated by solving a combined momentum equation. A no-slip boundary condition was used for the fins and projectile base as well. However, the value of the wall pressure was computed from a zero-order flow field extrapolation. Free-stream boundary conditions are used at the in-flow boundary as well as at the outer boundary. A symmetry boundary condition is imposed at the circumferential edges of the grid, while a simple extrapolation is used at the downstream boundary. A combination of symmetry and extrapolation boundary condition is used at the center line (axis). If the free-stream flow is supersonic, a nonreflection boundary condition can be used at the outer boundary. For the transonic Mach number of 0.95 for this case, it was necessary to use free-stream boundary conditions at the outer boundary. In order to impose free-stream boundary conditions, the outer boundary of the computational grid was placed approximately 20 calibers above the body surface. This distance was ascertained to be sufficient for ensuring that flow field disturbances created by the projectile did not propagate to the outer boundary.

3. MODEL GEOMETRY AND COMPUTATIONAL GRID

The model is a fairly simple high length-to-diameter ratio finned projectile. Only one-half of the total geometry needed to be modeled because of the inherent symmetry of the

6

case. The computational grid consists of 10 zones. The total number of points required to model the geometry was 2.5 million. As stated earlier, the Chimera technique was used in order to keep the grid density high near the projectile and fin surfaces while reducing the number of excess grid points in regions of smooth continuous air flow. The cylindrical portion of the body is a good example of such a region. The reduction in the number of grid points is evident in the manner in which the points are distributed in the circumferential direction. On the projectile ogive, cylinder, and base, 92 circumferential planes are used. This is all that is required for moderate angles of attack. However, in the fin region, more circumferential planes are required because of the heavy grid point clustering needed to ensure that an accurate viscous solution is achieved for each fin surface. In the computational zones used to model the area between the fins, 186 circumferential planes are used. The additional planes are especially useful for computing flow fields for large angles of attack where the transonic flow field generated by the fins becomes increasingly complex. Since the Chimera technique is employed, a point-to-point match between grids surrounding the fins and the grids used to model the relatively simple cylinder and base regions is not necessary. Thus, a high circumferential grid density can be employed in the fin region while an equally spaced circumferential grid can be used elsewhere. In a similar manner, the region near the fin tips is clustered, but the number of additional points required to accurately model the flow field about the fin tip is only reflected in the point total of the grids in direct contact with the fin surfaces. Figures 1 and 2 are cutaway views of the computational grid. The grid is color coded to differentiate between the forebody, fin, and base regions of the projectile. The red and dark blue regions each have 92 equally spaced circumferential planes. The light blue region is highly clustered in the circumferential direction and encompasses the fins. The Chimera scheme is employed in two places. The first location is just upstream from the fins and is depicted in Figures 1 and 2 as the position where the red region meets the light blue region. The second location is at the base of the projectile and is depicted in Figures 1 and 2 as the position where the light blue region meets the dark blue region.

4. RESULTS

Steady state calculations have been performed to numerically simulate the flow field about a finned projectile at moderate angles of attack. The computations were run at $M_\infty = 0.95$ at $\alpha = 2°$ and $\alpha = 10°$ at atmospheric flight conditions for an altitude of 200 m. These calculations required 91 million words of memory, and each case required approximately 70 hours of computer processor time on a Cray C-90 supercomputer.
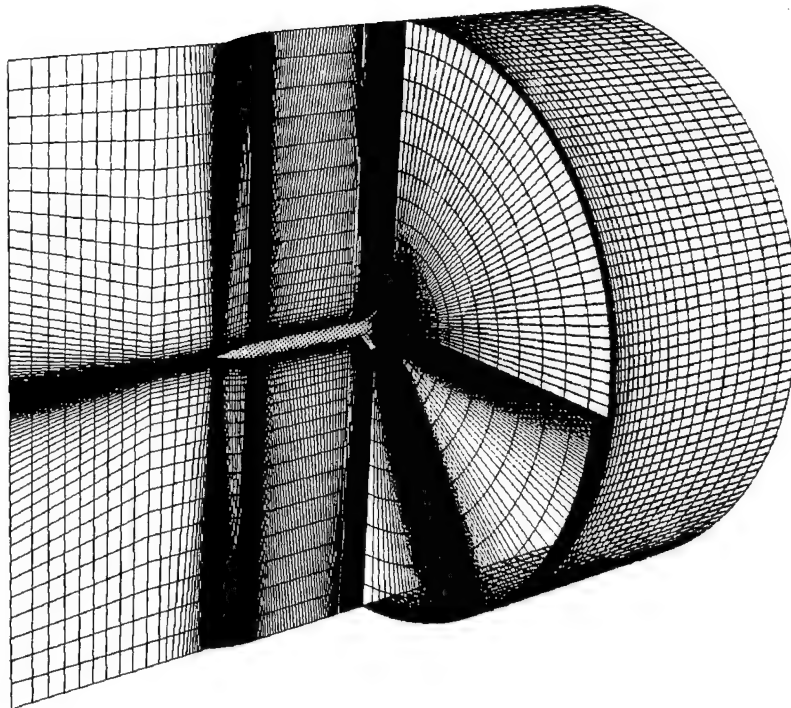
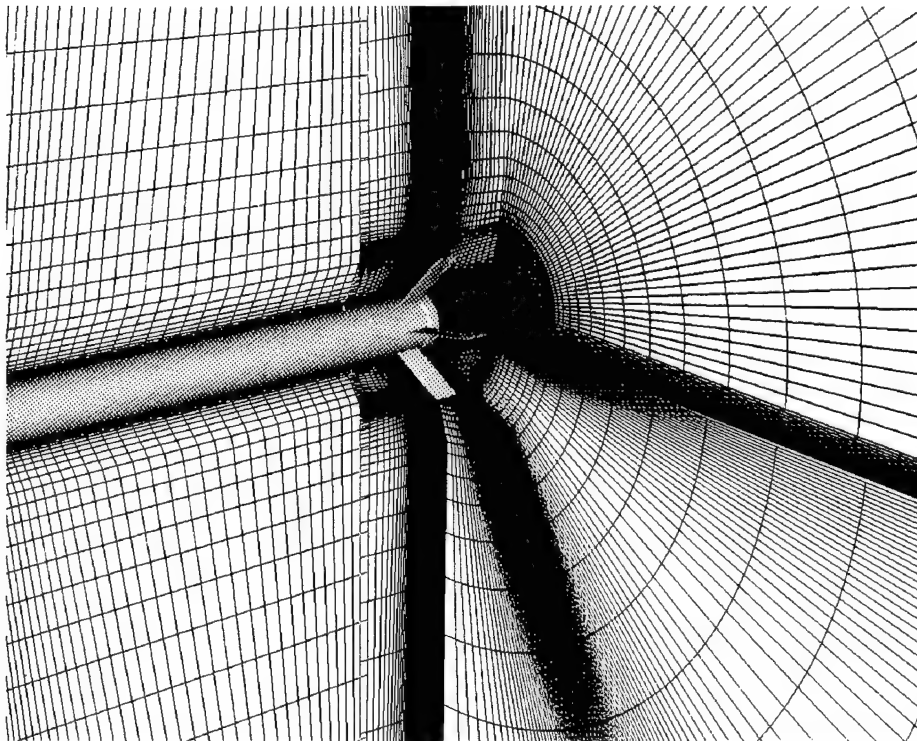Figure 1. Cutaway View of Complete Numerical Grid.

Figure 2. Closeup of Cutaway View of Numerical Grid.

8

Results are shown for both $2°$ and $10°$ angles of attack. Figures 3 and 4 show the symmetry-plane flow field Mach number contours for the entire projectile, while Figures 5 and 6 show a close-up of the base region symmetry-plane flow field Mach contours with particle traces superimposed over the contours. Subtle differences can be observed in the flow fields between the $2°$ and $10°$ cases. Most notable are the differences in contours over the cylindrical portion of the body and the differences in contours in the wake region. The particle traces demonstrate the 3-D complexity of the wake flow field. Since the wake is unsteady, it is difficult to draw any conclusion from a visual comparison between the contours of the $2°$ and $10°$ cases. Figures 7 and 8 show the symmetry-plane flow field pressure contours for the entire projectile. The flow field pressure contours for the $2°$ and $10°$ cases show relatively high pressure at the nose and a shock at the ogive-cylinder junction. As expected, these features appear more symmetric for the $2°$ case. For both the $2°$ and $10°$ cases, there is flow expansion at the point just aft of the fins where there is an increase in the body radius. Closely following is the recompression, which is more evident when viewing the Mach contours. The most notable difference between the $2°$ and $10°$ pressure contours occurs on the wind side, underneath of the projectile between the fins. The pressure appears to be somewhat higher for the $10°$ case than the $2°$ case in this region. This region of the flow field is partially obscured by the lowermost fin, but it is still quite visible. Figures 9 and 10 show the projectile surface pressure contours. From the wind side viewpoint, one can see the high pressure regions for the $10°$ case, which have developed on the ogive and on the body in the fin region. Figures 11 and 12 show the projectile surface pressure contours from the lee side viewpoint. From this perspective, the differences in surface pressure between the fins of the $2°$ and $10°$ cases are quite evident.

Figures 13 and 14 are pressure contours at the base of the projectile. From this perspective, the difference in surface pressure between the $2°$ and $10°$ cases on the base of the projectile is visible. Also, the difference in the fin wake flow field between the $2°$ and $10°$ cases is quite prominent. Overall, the contours indicate that a very complex 3-D flow field is produced by this projectile configuration. Although the flow field about the forebody is fairly simple, the flow field generated in the fin and wake region is very complex. The wake has a complicated structure with multiple recirculating flow cells for both the $2°$ and $10°$ cases.
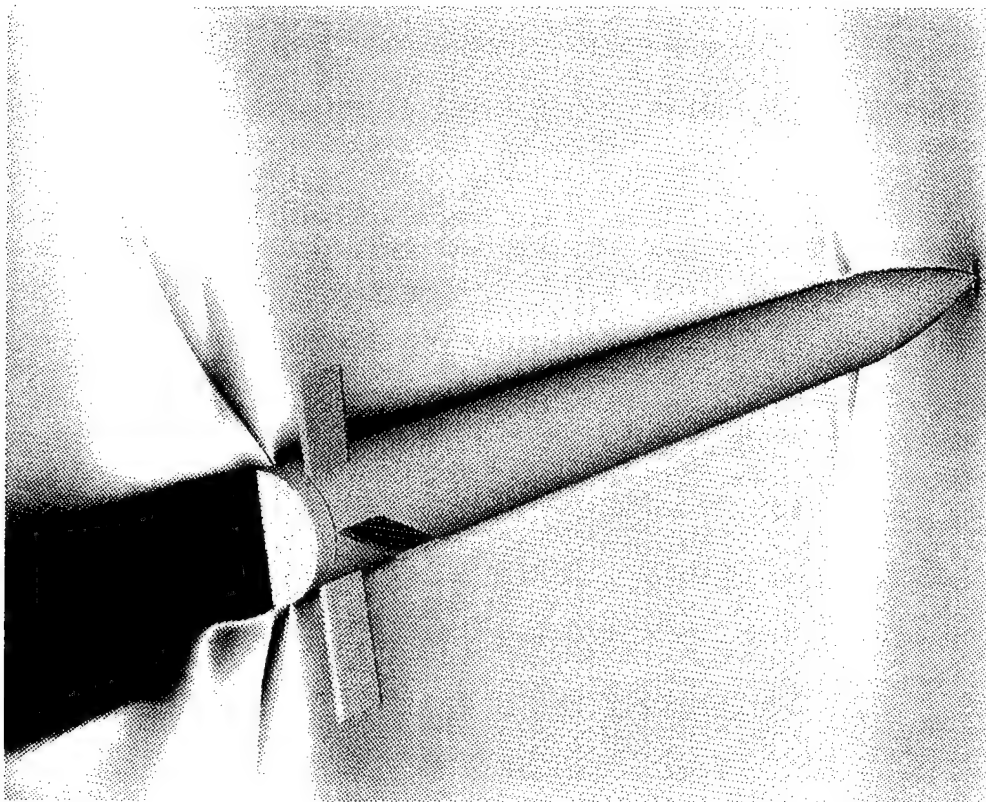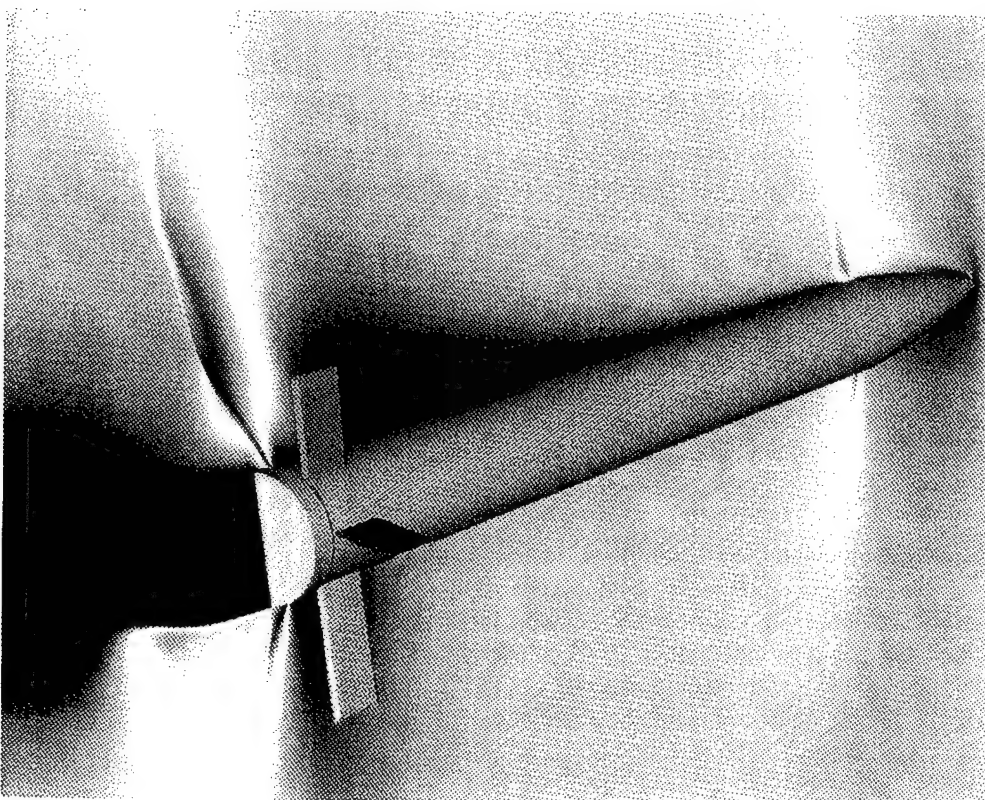
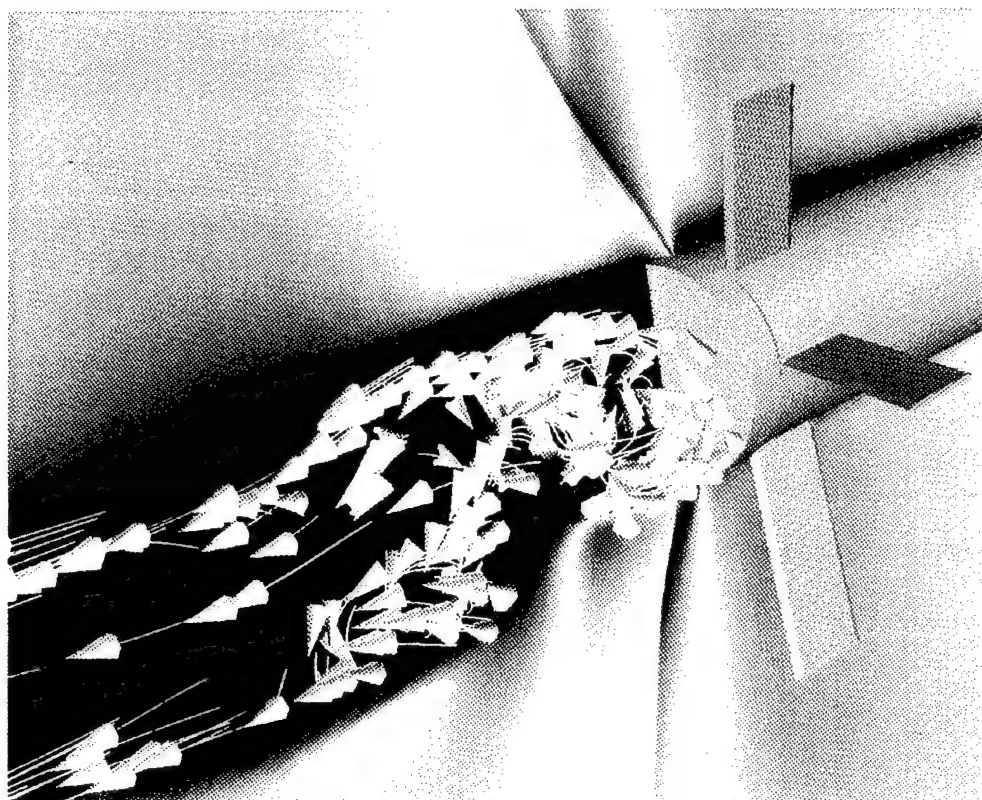Figure 3. Mach Contours on Symmetry Plane, $\alpha = 2°$.

1.80
1.35
0.90
0.45
0.00

Figure 4. Mach Contours on Symmetry Plane, $\alpha = 10°$.

Figure 5. Mach Contours and Particle Traces on Symmetry Plane, $\alpha = 2^\circ$.
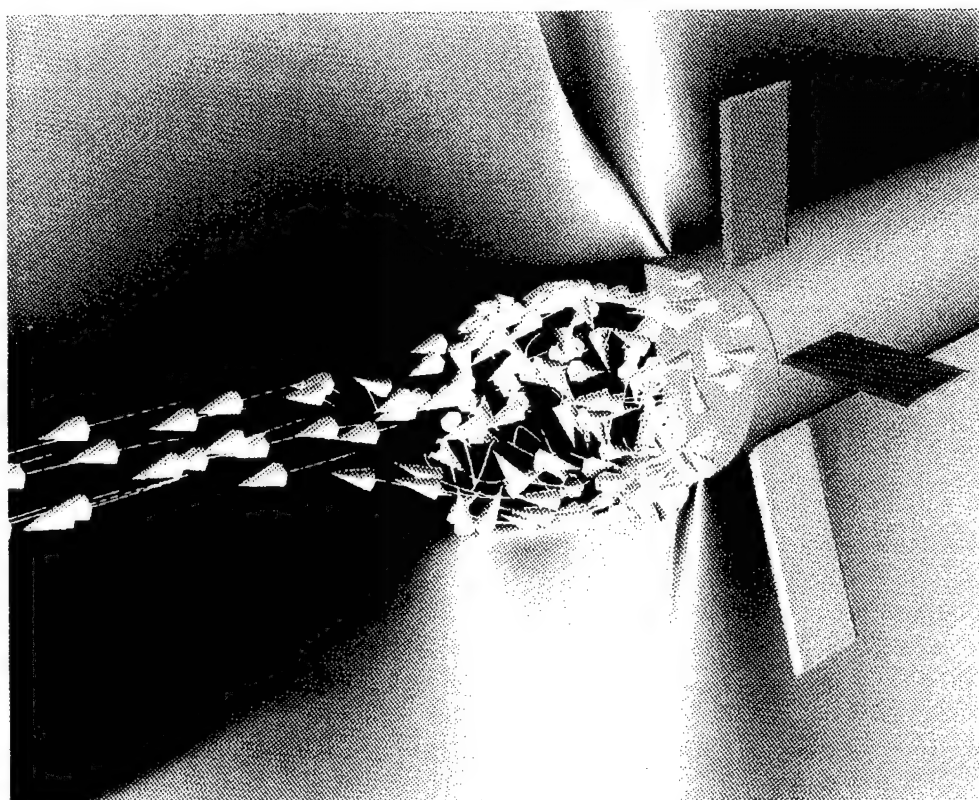
1.80
1.35
0.90
0.45
0.00
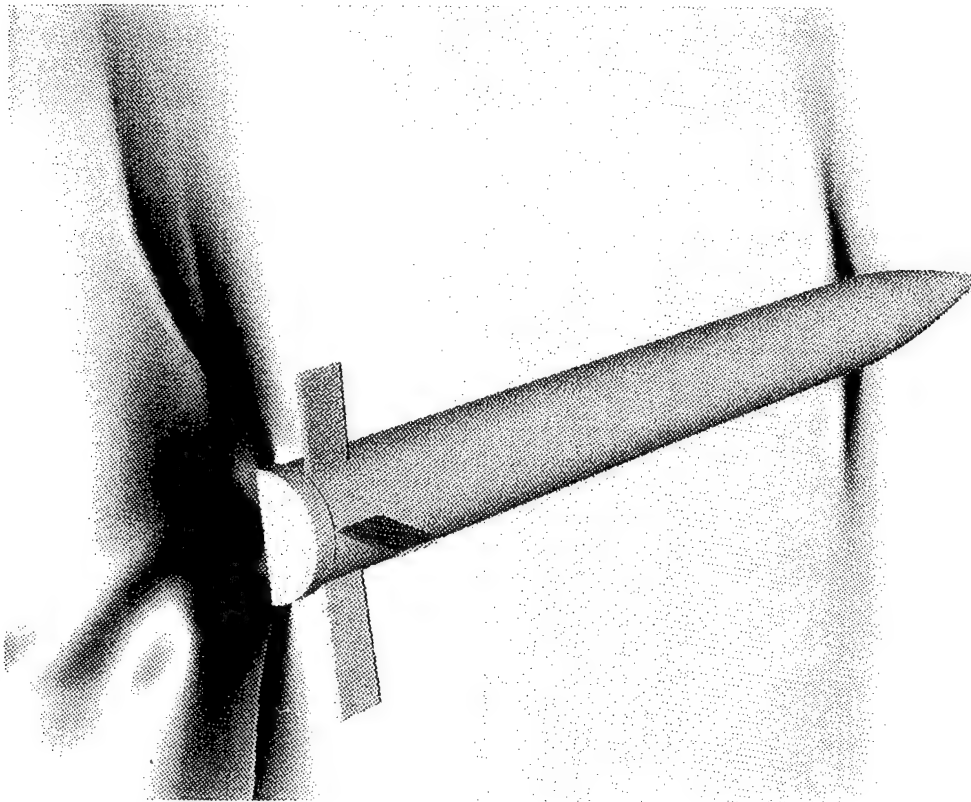

Figure 6. Mach Contours and Particle Traces on Symmetry Plane, $\alpha = 10^\circ$.

Figure 7. Normalized Pressure Contours on Symmetry Plane, $\alpha = 2^\circ$.
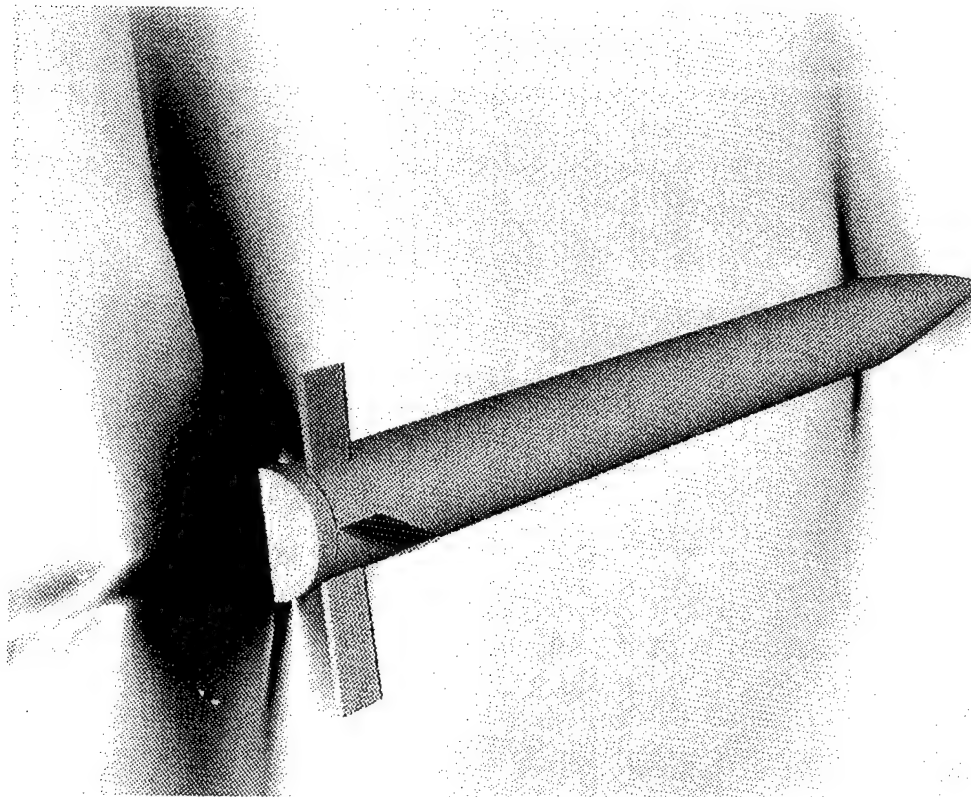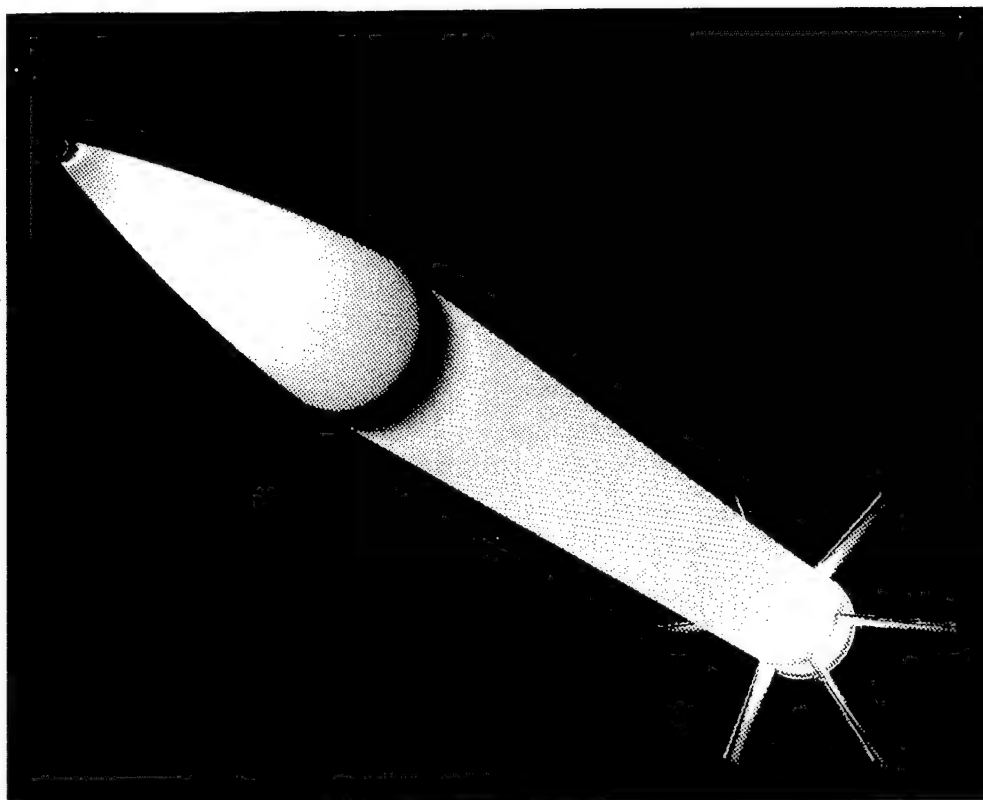
1.30
1.05
0.80
0.55
0.30
0.05

Figure 8. Normalized Pressure Contours on Symmetry Plane, $\alpha = 10^\circ$.

Figure 9. Normalized Pressure Contours, Wind Side Viewpoint, $\alpha = 2°$.

1.30
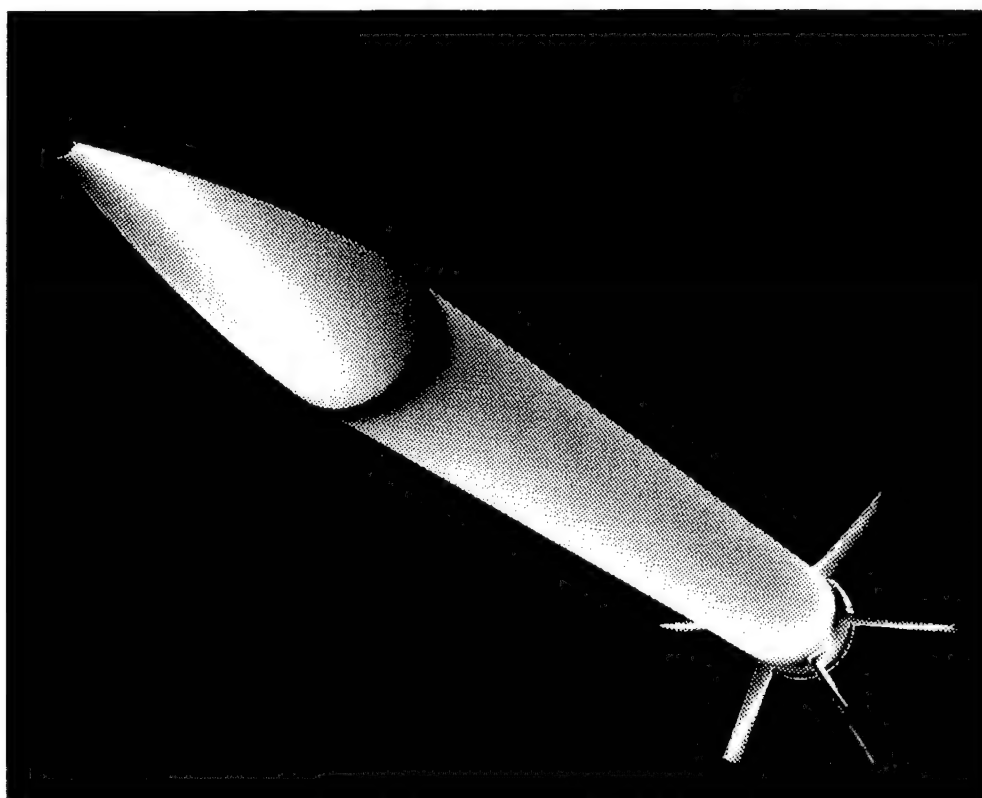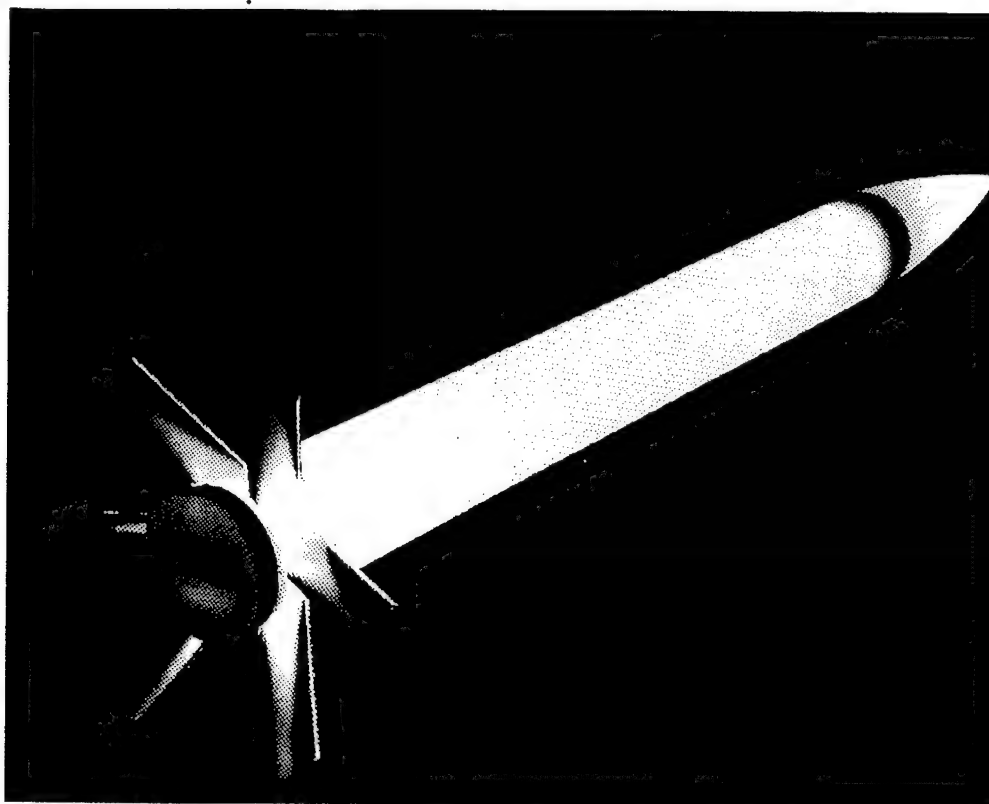1.05
0.80
0.55
0.30
0.05

Figure 10. Normalized Pressure Contours, Wind Side Viewpoint, $\alpha = 10°$.

13

Figure 11. Normalized Pressure Contours, Lee Side Viewpoint, $\alpha = 2°$.

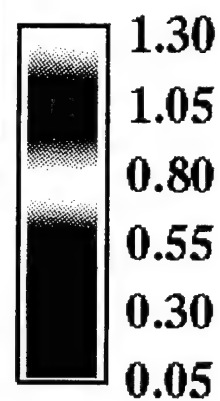|	
	1.30
	1.05
	0.80
	0.55
	0.30
	0.05

Figure 12. Normalized Pressure Contours, Lee Side Viewpoint, $\alpha = 10°$.
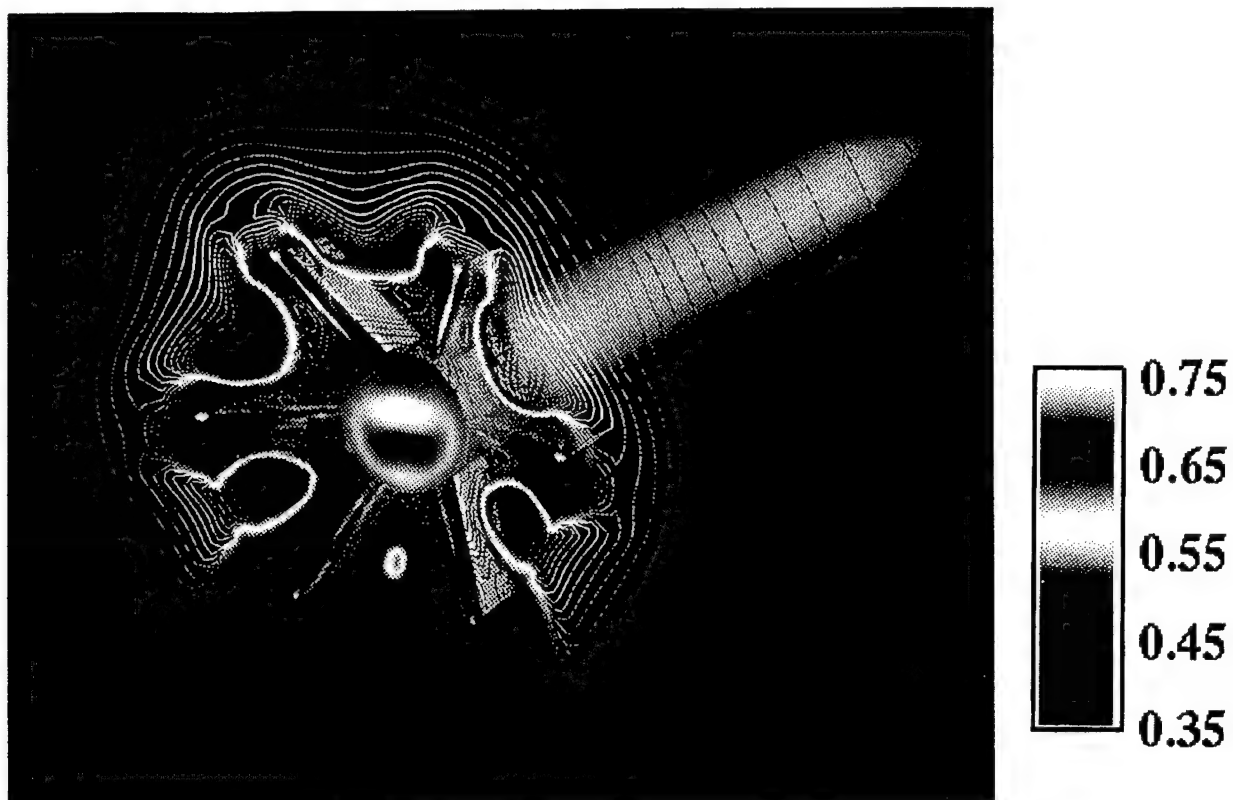
14

Figure 13. Normalized Pressure Contours, Projectile Base and Fin Wake, $\alpha = 2^\circ$.
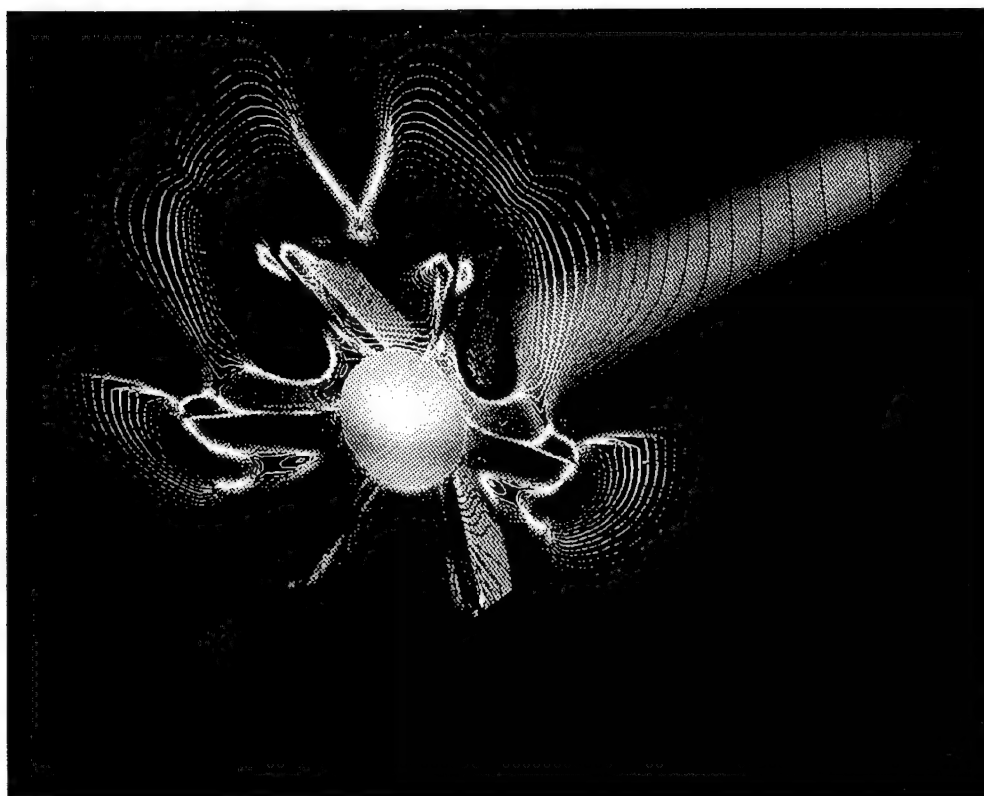

Figure 14. Normalized Pressure Contours, Projectile Base and Fin Wake, $\alpha = 10^\circ$.

Aerodynamic coefficients computed from the CFD solutions were compared with aerodynamic coefficients computed by an empirical missile aerodynamics design code, AP95 (see Moore, McInville, and Hymer 1995a & b), for a Mach number of 0.95. Table 1 lists the data for an angle of attack at $\alpha = 2°$, and Table 2 lists the data for $\alpha = 10°$. It is difficult to obtain accurate aerodynamic coefficients within the transonic regime for numerical comparison. Although there is some difference in the magnitude of the aerodynamic coefficients obtained from each code, the comparison between the aerodynamic coefficients obtained from F3D and AP95 indicates that the results obtained from F3D basically follow the same aerodynamic trends encoded within AP95. The drag coefficient and $C_{m\alpha}$ increase as the angle of attack increases, while $C_{N\alpha}$ and Xcp decrease with an increase in angle of attack. However, the aerodynamic coefficients themselves are somewhat different. It is difficult to pinpoint the source of the inconsistency between the data provided by AP95 and F3D. At this point, please note that there were some differences in the geometric model used in AP95 and F3D. The geometric model used by AP95 was simplified from the model used in the F3D computations in that it did not include a small increase in the body radius aft of the fin section, which was included to model a possible obturator design. Such a detail is not usually modeled with a design code. Instead, the AP95 geometric model had a constant radius cylinder for the entire body aft of the ogive. The increase in radius was abrupt, and the CFD computations indicate a shock at the point where the radius increases. Also, the increase in body radius translates into an increase in the base area of the body. The F3D geometric model had a 10.6% greater base area than the geometric model used for the AP95 computations. Overall, the geometric differences were small, and it should not be implied that the difference in the geometric model is the sole factor responsible for the differences in the aerodynamic coefficients computed.

Table 1. Force and Moment Coefficient Data for $\alpha = 2°$

$\alpha = 2°$	F3D	AP95
Cd	0.694	0.499
$C_{N\alpha}$	16.693	13.50
$C_{m\alpha}$	-63.75	-40.31
Xcp	3.82	2.98

Table 2. Force and Moment Coefficient Data for $\alpha = 10°$

$\alpha = 10°$	F3D	AP95
Cd	1.145	0.837
$C_{N\alpha}$	16.052	12.17
$C_{m\alpha}$	-58.85	-31.19
Xcp	3.66	2.56

5. CONCLUDING REMARKS

Predictions for the aerodynamic coefficients of a proposed U.S. Army projectile were obtained using the F3D zonal, thin layer, Navier-Stokes code and the Chimera grid discretization technique. The aerodynamic coefficients were computed for a free stream velocity of Mach 0.95 at two angles of attack, $2°$ and $10°$. The Chimera technique allowed for high grid resolution in the fin region without placing unneeded grid points over the smooth, highly elongated body. The computed flow field captures intricate features of the air flow about the projectile. The F3D solution predicts a very complex projectile wake flow field for $2°$ and $10°$ angle of attack. Qualitatively, the flow field predicted at $2°$ angle of attack was substantially different from the flow field computed for $10°$ angle of attack. Aerodynamic coefficients were computed from the F3D flow field solutions and were compared with aerodynamic coefficients by the AP95 missile design code. Although the aerodynamic coefficient magnitudes were different, the data indicate that AP95 predicts similar changes in the aerodynamic coefficients as the angle of attack is varied. Computations at Mach 0.95, within the transonic region, are extremely sensitive, so the matching aerodynamic trends of AP95 and F3D coefficient data are encouraging. However, there is also clear indication that more work needs to be done to verify the predictions of aerodynamic coefficients of finned projectiles within the transonic velocity region. This initial effort has shown that the use of the Chimera technique to geometrically model finned projectiles is promising for future computations.

INTENTIONALLY LEFT BLANK

6. REFERENCES

Baldwin, B. S., and H. Lomax. "Thin Layer Approximation and Algebraic Model for Separated Turbulent Flows." AIAA Paper No. 78-257, American Institute for Astronautics and Aeronautics, January 1978.

Benek J. A., T. L. Donegan, and N. E. Suhs. "Extended Chimera Grid Embedding Scheme with Application to Viscous Flows." AIAA Paper No. 87-1126-CP, American Institute for Astronautics and Aeronautics, 1987.

Meakin, R. L., and N. Suhs. "Unsteady Aerodynamic Simulation of Multiple Bodies in Relative Motion." AIAA 9th Computational Fluid Dynamics Conference, AIAA Paper No. 89-1996, American Institute for Astronautics and Aeronautics, June 1989.

Moore, F. G., R. M. McInville and T. C. Hymer. "The 1995 Version of the NSWC Aeroprediction Code: Part I - Summary of New Theoretical Methodology." NSWCDD/TR-94/379, February 1995.

Moore, F. G., R. M. McInville and T. C. Hymer. "The 1995 Version of the NSWC Aeroprediction Code: Part II - Computer Program Users Guide and Listing." NSWCDD/TR-94, March 1995.

Pulliam, T. H., and J. L. Steger. "On Implicit Finite-Difference Simulations of Three-Dimensional Flow." *AIAA Journal*, vol. 18, no. 2, pp. 159–167, February 1982.

Steger, J. L., S. X. Ying, and L. B. Schiff. "A Partially Flux-Split Algorithm for Numerical Simulation of Compressible Inviscid and Viscous Flows." *Proceedings of the Workshop on Computational Fluid Dynamics*, Institute of Nonlinear Sciences, University of California, Davis, CA, 1986.

INTENTIONALLY LEFT BLANK

7. BIBLIOGRAPHY

Atta, E. H., and J. Vadyak. "A Grid Interfacing Zonal Algorithm for Three-Dimensional Flow Transonic Flows About Aircraft Configurations." AIAA Paper No. 82-1017, American Institute for Astronautics and Aeronautics, 1982.

Buning, P. G., I. T. Chiu, S. Obayashi, Y. M. Rizk, and J. L. Steger. "Numerical Simulation of the Integrated Space Shuttle Vehicle in Ascent." American Institute for Astronautics and Aeronautics, Atmospheric Flight Mechanics Conference, August 1988.

Sahu, J. "Computations of Supersonic Flow Over a Missile Afterbody Containing an Exhaust Jet." *AIAA Journal of Spacecraft and Rockets*, vol. 24, no. 5, pp. 403–410, September–October 1987.

Sahu, J. "Numerical Computations of Transonic Critical Aerodynamic Behavior." *AIAA Journal*, vol. 28, no. 5, pp. 807–816, May 1990 (also see BRL-TR-2962, December 1988).

Sahu, J., and C. J. Nietubicz. "Application of Chimera Technique to Projectiles in Relative Motion." ARL-TR-590, U.S. Army Research Laboratory, Aberdeen Proving Ground, MD, October 1994.

Sahu, J., C. J. Nietubicz, and J. L. Steger. "Navier-Stokes Computations of Projectile Base Flow With and Without Base Injection." *AIAA Journal*, vol. 23, no. 9, pp. 1348–1355, September 1985.

Sahu, J., and J. L. Steger. "Numerical Simulation of Three-Dimensional Transonic Flows." AIAA Paper No. 87-2293, American Institute for Astronautics and Aeronautics, Atmospheric Flight Mechanics Conference, Monterey, CA, August 1987.

Steger, J. L., F. C. Dougherty, and J. A. Benek. "A Chimera Grid Scheme." Advances in Grid Generation, ASME FED-5, K. N. Ghia and U. Ghia (eds.), June 1983.

INTENTIONALLY LEFT BLANK

NO. OF COPIES	ORGANIZATION	NO. OF COPIES	ORGANIZATION
2	ADMINISTRATOR DEFENSE TECHNICAL INFO CENTER ATTN DTIC DDA 8725 JOHN J KINGMAN RD STE 0944 FT BELVOIR VA 22060-6218	1	CDR NSWC CODE B40 DR W YANTA DAHLGREN VA 22448-5100
1	DIRECTOR US ARMY RESEARCH LABORATORY ATTN AMSRL CS AL TA RECORDS MANAGEMENT 2800 POWDER MILL RD ADELPHI MD 20783-1197	1	CDR NSWC CODE 420 DR A WARDLAW INDIAN HEAD MD 20640-5035
		1	CDR NSWC ATTN DR F MOORE DAHLGREN VA 22448
1	DIRECTOR US ARMY RESEARCH LABORATORY ATTN AMSRL CI LL TECHNICAL LIBRARY 2800 POWDER MILL RD ADELPHI MD 207830-1197	1	NAVAL AIR WARFARE CENTER ATTN DAVID FINDLAY MS 3 BLDG 2187 PATUXENT RIVER MD 20670
1	DIRECTOR US ARMY RESEARCH LABORATORY ATTN AMSRL CS AL TP TECH PUBLISHING BRANCH 2800 POWDER MILL RD ADELPHI MD 20783-1197	4	DIR NASA LANGLEY RESEARCH CENTER ATTN TECH LIBRARY MR D M BUSHNELL DR M J HEMSCH DR J SOUTH LANGLEY STATION HAMPTON VA 23665
7	CDR US ARMY ARDEC ATTN AMSTE AET A R DEKLEINE C NG R BOTTICELLI H HUDGINS J GRAU S KAHN W KOENIG PICATINNY ARSENAL NJ 07806-5001	2	ARPA ATTN DR P KEMMEY DR JAMES RICHARDSON 3701 NORTH FAIRFAX DR ARLINGTON VA 22203-1714
1	CDR US ARMY ARDEC ATTN AMSTE CCH V PAUL VALENTI PICATINNY ARSENAL NJ 07806-5001	7	DIR NASA AMES RESEARCH CENTER MS 227 8 L SCHIFF MS 258 1 T HOLST MS 258 1 D CHAUSSEE MS 258 1 M RAI MS 258 1 P KUTLER MS 258 1 P BUNING MS 258 1 B MEAKIN MOFFETT FIELD CA 94035
1	CDR US ARMY ARDEC ATTN SFAE FAS SD MIKE DEVINE PICATINNY ARSENAL NJ 07806-5001		
2	USAF WRIGHT AERONAUTICAL LABS ATTN AFWAL FIMG DR J SHANG MR N E SCAGGS WPAFB OH 45433-6553	2	USMA DEPT OF MECHANICS ATTN LTC ANDREW L DULL M COSTELLO WEST POINT NY 10996
3	AIR FORCE ARMAMENT LAB ATTN AFATL/FXA STEPHEN C KORN BRUCE SIMPSON DAVE BELK EGLIN AIR FORCE BASE FL 32542-5434	2	UNIV OF CALIFORNIA DAVIS DEPT OF MECHANICAL ENGRG ATTN PROF H A DWYER PROF M HAFEZ DAVIS CA 95616

NO. OF
COPIES   ORGANIZATION

        AMSRL WM WB   F BRANDON
                T BROWN   W D'AMICO
                B DAVIS   E FERGUSON
                M HOLLIS
        AMSRL WM TB   R LOTTERO
        AMSRL CI H   C NIETUBICZ
        AMSRL CI HC   P COLLINS
                D HISLEY   D PRESSEL
                W STUREK

INTENTIONALLY LEFT BLANK

REPORT DOCUMENTATION PAGE

Public reporting burden for this collection of information is estimated to average 1 hour per response, including the time for reviewing instructions, searching existing data sources, gathering and maintaining the data needed, and completing and reviewing the collection of information. Send comments regarding this burden estimate or any other aspect of this collection of information, including suggestions for reducing this burden, to Washington Headquarters Services, Directorate for Information Operations and Reports, 1215 Jefferson Davis Highway, Suite 1204, Arlington, VA 22202-4302, and to the Office of Management and Budget, Paperwork Reduction Project (0704-0188), Washington, DC 20503.

1. AGENCY USE ONLY *(Leave blank)*	2. REPORT DATE December 1997	3. REPORT TYPE AND DATES COVERED Final

4. TITLE AND SUBTITLE

Computational Modeling of a Finned Projectile by Chimera Technique

5. FUNDING NUMBERS

PR: 1L1611102AH43

6. AUTHOR(S)

Edge, H.L.; Sahu, J. (both of ARL)

7. PERFORMING ORGANIZATION NAME(S) AND ADDRESS(ES)

U.S. Army Research Laboratory
Weapons & Materials Research Directorate
Aberdeen Proving Ground, MD 21010-5066

8. PERFORMING ORGANIZATION REPORT NUMBER

9. SPONSORING/MONITORING AGENCY NAME(S) AND ADDRESS(ES)

U.S. Army Research Laboratory
Weapons & Materials Research Directorate
Aberdeen Proving Ground, MD 21010-5066

10. SPONSORING/MONITORING AGENCY REPORT NUMBER

ARL-TR-1443

11. SUPPLEMENTARY NOTES

12a. DISTRIBUTION/AVAILABILITY STATEMENT

Approved for public release; distribution is unlimited.

12b. DISTRIBUTION CODE

13. ABSTRACT *(Maximum 200 words)*

A computational study was performed to compute the aerodynamic coefficients of a long-range finned projectile configuration at a transonic velocity of Mach 0.95 for multiple angles of attack. A zonal, implicit, Navier-Stokes computational technique, along with the Chimera overset grid approach, has been used to compute the projectile flow field. The application of the Chimera approach allowed for improved efficiency in terms of placing grid points where they are needed the most. This technique is promising for future flow field computations of finned projectiles. The aerodynamic coefficients computed are then compared with those computed through application of a design code to show comparable results.

14. SUBJECT TERMS

computational fluid dynamics   finned projectile   three-dimensional
Chimera technique   Navier-Stokes

15. NUMBER OF PAGES
37

16. PRICE CODE

17. SECURITY CLASSIFICATION OF REPORT Unclassified	18. SECURITY CLASSIFICATION OF THIS PAGE Unclassified	19. SECURITY CLASSIFICATION OF ABSTRACT Unclassified	20. LIMITATION OF ABSTRACT